



Article

Fast Algorithm of Passive Bistatic Radar Detection Based on Batches Processing of Sparse Representation and Recovery

Kai Cui ¹ , Changlong Wang ^{1,*}, Feng Zhou ¹, Chunheng Liu ¹, Yongchan Gao ¹ and Weike Feng ²

¹ Key Laboratory of Electronic Information Countermeasure and Simulation Technology, Ministry of Education, Xidian University, Xi'an 710071, China; cuikai7308@163.com (K.C.); fzhou@mail.xidian.edu.cn (F.Z.); lchxidian@126.com (C.L.); ycgao@xidian.edu.cn (Y.G.)

² Air Defense and Antimissile School, Air Force Engineering University, Xi'an 710051, China; fengweike007@163.com

* Correspondence: clw_xjtu@163.com

Abstract: In the passive bistatic radar (PBR) system, methods exist to address the issue of detecting weak targets without being influenced by non-ideal factors from adjacent strong targets. These methods utilize the sparsity in the delay-Doppler domain of the cross ambiguity function (CAF) to detect weak targets. However, the modeling and solving of this method involve substantial memory consumption and computational complexity. To address these challenges, this paper establishes a target detection model for PBR based on batch processing of sparse representation and recovery. This model partitions the CAF into blocks, identifies blocks requiring processing based on the presence of targets, and improves the construction and utilization of the measurement matrix. This results in a reduction in the computational complexity and memory resource requirements for sparse representation and recovery, and provides favorable conditions for parallel execution of the algorithm. Experimental results indicate that the proposed approach increases the number of blocks by a factor of four, and reduces the number of real multiplications by approximately an order of magnitude. Hence, compared with the traditional approach, the proposed approach enables fast and stable detection of weak targets.

Keywords: passive bistatic radar (PBR); cross ambiguity function (CAF); sparse representation; sparse recovery; fast calculation



Citation: Cui, K.; Wang, C.; Zhou, F.; Liu, C.; Gao, Y.; Feng, W. Fast Algorithm of Passive Bistatic Radar Detection Based on Batches Processing of Sparse Representation and Recovery. *Remote Sens.* **2024**, *16*, 2294. <https://doi.org/10.3390/rs16132294>

Academic Editor: Dusan Gleich

Received: 30 April 2024

Revised: 5 June 2024

Accepted: 18 June 2024

Published: 23 June 2024



Copyright: © 2024 by the authors. Licensee MDPI, Basel, Switzerland. This article is an open access article distributed under the terms and conditions of the Creative Commons Attribution (CC BY) license (<https://creativecommons.org/licenses/by/4.0/>).

1. Introduction

Passive bistatic radar (PBR) is a radar system that operates in a receive-only mode. It detects and tracks targets by utilizing signals emitted from illuminators of opportunity (IOs) [1,2]. In the conventional PBR system using correlation detection, signal processing operations are performed, including reference signal purification [3], clutter cancellation [4,5], and cross ambiguity function (CAF) computation [6]. The peak of CAF reflects the bistatic time delay and Doppler frequency, corresponding to the target's position and velocity information [7]. As PBR receives signals from IOs and has a separated transmitter–receiver structure, it possesses advantages such as interference resistance, anti-stealth capabilities, resistance to low-altitude penetration, cost-effectiveness and efficient spectrum utilization. Common IOs include frequency modulation (FM) [8], digital audio broadcasting (DAB) [9], digital video broadcasting terrestrial (DVB-T) [10], digital terrestrial multimedia broadcasting (DTMB) [11], digital video broadcasting satellite (DVB-S) [12], global system for mobile communications (GSM) [13], beidou navigation satellite system (BDS) [14], global positioning system (GPS) [15], and so on. However, as these signals are not specifically designed for PBR, their ambiguity functions do not exhibit a spike-like nature. As shown in Figure 1, taking DVB-T, DTMB, and 5th generation mobile communication technology (5G) downlink signals as examples, their ambiguity functions show mainlobe and sidelobe widening. Additionally, due to the special frame structures of these signals, there are side

peaks in the ambiguity functions [16–18]. These non-ideal factors pose challenges in the weak targets detection.

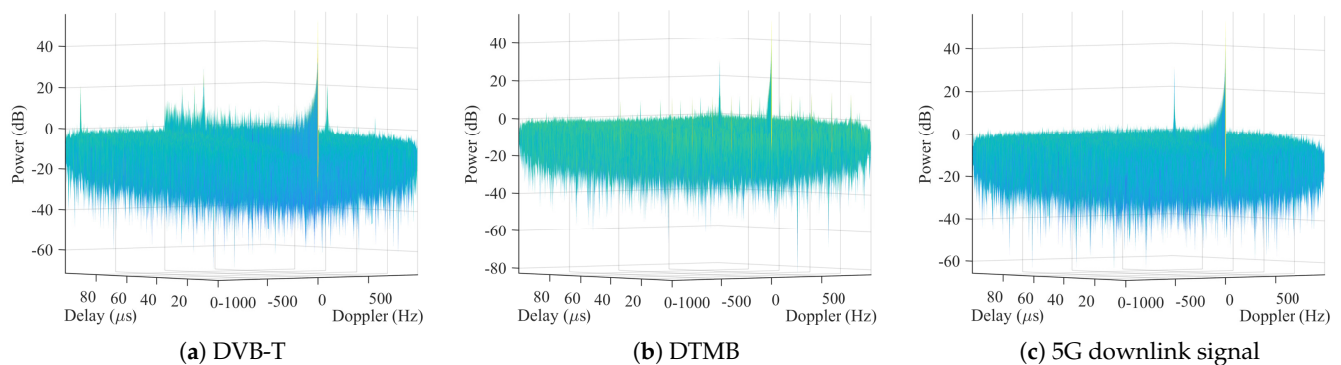


Figure 1. The ambiguity function properties of different signals are not ideal spike-like. (a) DVB-T. (b) DTMB. (c) 5G downlink signal.

Sparse representation and recovery techniques have been widely applied in various fields such as communication [19–21], image [22–24], and radar [25–27]. In the field of PBR, the two technologies are utilized for weak target detection. Among them, the authors of [28,29] applied sparse representation and recovery techniques to PBR target detection. However, their models relied on the orthogonality between subcarriers of orthogonal frequency-division multiplexing (OFDM) and the cyclic prefix of OFDM symbols. As a result, the applicable types of signals were limited. References [30–35] utilised the sparsity of surveillance signals in the delay-Doppler domain for the sparse recovery of CAF. These approaches based on this idea have the characteristic of wide applicability and have been widely adopted. Based on the source of the measurement matrix, the research results based on this idea can be classified into the following categories: (1) The measurement matrix is constructed by adding different delays and Doppler frequencies to the reference signal [30–33]. (2) Based on the computation of CAF, the Doppler-shifted Fourier transform matrix is derived as the measurement matrix [34]. (3) The measurement matrix consists of CAFs with different delays and Doppler frequencies [35]. Among these, Method (1) has a simple construction of the measurement matrix and a lower computational complexity. However, it demands a higher signal-to-noise ratio (SNR) for the surveillance signal, resulting in a poor detection performance for weak targets. Method (2) exhibits a better detection performance for weak targets than Method (1) because of coherent accumulation. In this method, it divides the signal into multiple batches and randomly utilizes some of them. In this way, memory resources and computational complexity are saved. However, utilization of the Doppler dimension is reduced, lowering the detection performance for weak targets. Although Method (3) achieves the best detection performance for weak targets among the three methods, its measurement matrix has a large scale. So, the requirements of memory resources is hard to guarantee. Additionally, each sample of the measurement matrix needs to be calculated through the computation of CAF by adding delays and Doppler frequencies to the reference signal. Hence, this method consumes a significant amount of computational resources during the measurement matrix construction stage, affecting the real-time performance.

Therefore, this paper proposes a target detection method for PBR based on batches processing of sparse representation and recovery. This method partitions CAF into blocks, selects blocks that contain targets, and improves the construction and utilization of the measurement matrix. Compared with Method (3), this method maintains the detection performance for weak targets while reducing the memory resource and computational requirements. Hence, this method provides favorable conditions for the parallel execution. The effectiveness of this method is validated in the experimental results.

2. Signal Model

The schematic diagram of the idealized PBR system is shown in Figure 2. The system has two antennas to receive the reference signal and surveillance signal, respectively.

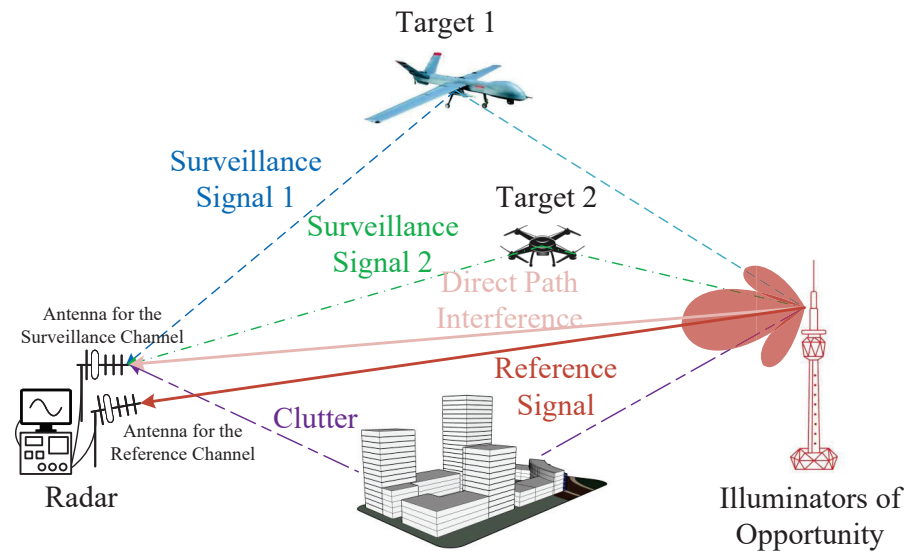


Figure 2. The schematic diagram of the idealized PBR system.

In a PBR system, the idealized baseband reference signal $u_{ref}(t)$ comprises two components: the baseband signal from IO and noise. Its expression is given by

$$u_{ref}(t) = A_{ref}u(t - \tau_0) + n_{ref}(t) \quad (1)$$

where A_{ref} is the amplitude of the reference signal, $u(t)$ is the baseband signal from the IO, τ_0 is the time delay between IO and radar, and $n_{ref}(t)$ is the noise in the reference channel.

The baseband surveillance signal $u_{surv}(t)$ received by radar comprises four components: the reference signal component, multipath clutter, target echo, and noise. Its expression is given by

$$u_{surv}(t) = A_{surv}u(t - \tau_0) + \sum_{k=1}^K A_k u(t - \tau_k) + \sum_{p=1}^P A_p u(t - \tau_p) e^{j2\pi f_p t} + n_{surv}(t) \quad (2)$$

where A_{surv} is the amplitude of the reference signal component; K is the number of multipath clutter components; A_k is the amplitude of the k -th multipath clutter; τ_k is the time delay of the k -th multipath clutter; P is the number of targets; A_p is the amplitude of the p -th target echo, τ_p and f_p are the time delay and Doppler frequency of the p -th target echo, respectively; and $n_{surv}(t)$ represents the noise in the surveillance signal.

To obtain the position and velocity of the target, the PBR system suppresses the reference signal and multipath clutter components in the surveillance signal. Subsequently, it estimates the target's position and velocity by identifying the delay and Doppler frequency corresponding to the peak of the CAF. Let $u'_{surv}(t)$ represent the idealized surveillance signal with the reference signal and multipath clutter components suppressed. The expression is

$$u'_{surv}(t) = \sum_{p=1}^P A_p u(t - \tau_p) e^{j2\pi f_p t} + n_{surv}(t) \quad (3)$$

So the expression of CAF is

$$\begin{aligned} \chi(\tau, f_d) &= \int_0^T u_{ref}^*(t - \tau) u'_{surv}(t) e^{-j2\pi f_d t} dt \\ &= \sum_{p=1}^P A_{ref}^* A_p \chi_p(\tau, f_d) + n_\chi(\tau, f_d) \\ &= A_{ref}^* \sum_{p=1}^P A_p \int_0^T u^*(t - \tau_0 - \tau) u(t - \tau_p) e^{-j2\pi(f_d - f_p)t} dt + n_\chi(\tau, f_d) \end{aligned} \tag{4}$$

where τ and f_d are the delay and Doppler frequency, respectively; T is the integration time; $\chi_p(\tau, f_d)$ is the CAF of the p -th target; and $n_\chi(\tau, f_d)$ represents the impact of noise on the CAF calculation. Equation (4) indicates that the CAF between the reference signal and the surveillance signal can be represented as a linear combination of the CAFs between the reference signal and copies of itself with added delays and Doppler frequencies. This forms the basis for the sparse representation of CAF.

3. Fast Batches Processing of Sparse Representation and Recovery in Delay-Doppler Domain

3.1. Fast Batches Processing of Sparse Representation

In this section, we introduce the fast algorithm of batches processing of sparse representation and recovery in the delay-Doppler domain. The flowchart is shown in Figure 3. The steps of this algorithm are summarized at the end of this section.

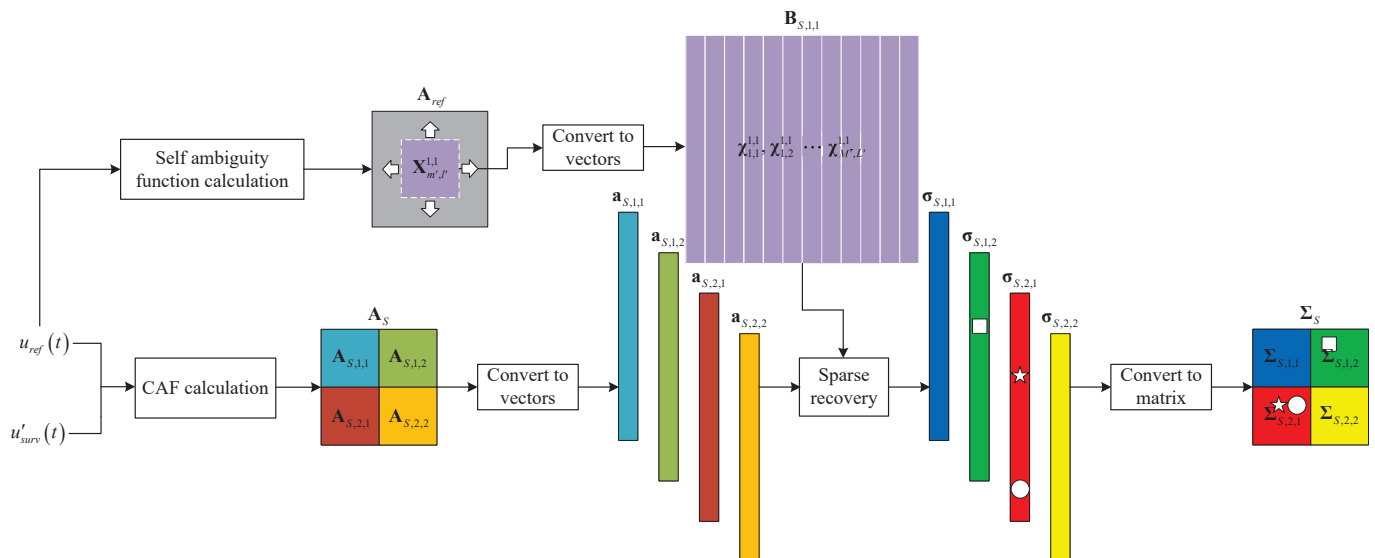


Figure 3. The flowchart for fast batches processing of sparse representation and recovery in the delay-Doppler domain.

To construct a sparse representation model for CAF, it is assumed that there could be a surveillance signal on each unit in the delay-Doppler domain. Let $\{\tau_1, \tau_2, \dots, \tau_L\}$, and $\{f_{d1}, f_{d2}, \dots, f_{dM}\}$ represent the sets of delay and Doppler frequency, respectively. Where L and M are the number of delay units and Doppler frequency units, respectively. The expression for CAF in (4) can be written as

$$\chi(\tau, f_d) = \sum_{m=1}^M \sum_{l=1}^L \sigma_{m,l} \chi_{m,l}(\tau, f_d) + n_\chi(\tau, f_d) \tag{5}$$

where $\sigma_{m,l}$ represents the amplitude gain under the delay τ_l and the Doppler frequency f_{dm} of the surveillance signal, and it can be expressed as

$$\sigma_{m,l} = \begin{cases} \frac{A_p}{A_{ref}}, (\tau_l, f_{dm}) = (\tau_p - \tau_0, f_p) \\ 0, \text{others} \end{cases} \tag{6}$$

$\chi_{m,l}(\tau, f_d)$ represents the CAF between the reference signal $u_{ref}(t)$ and a copy of itself with added delay and Doppler frequency $u_{ref}(t - \tau_l)e^{j2\pi f_{dm}t}$, and it can be expressed as

$$\chi_{m,l}(\tau, f_d) = \int_0^T u_{ref}^*(t - \tau)u_{ref}(t - \tau_l)e^{-j2\pi(f_d - f_{dm})t} dt \tag{7}$$

Let $\mathbf{a}_S \in \mathbb{C}^{LM \times 1}$ be a column vector formed by slicing and stacking the CAF $\chi(\tau, f_d)$ along each Doppler frequency unit, expressed as

$$\mathbf{a}_S = [\chi(\tau_1, f_{d1}) \chi(\tau_2, f_{d1}) \cdots \chi(\tau_L, f_{d1}) \chi(\tau_1, f_{d2}) \cdots \chi(\tau_1, f_{dM}) \cdots \chi(\tau_L, f_{dM})]^T \tag{8}$$

Different reference signal copies are generated by adding various delays and Doppler frequencies to the reference signal $u_{ref}(t)$. These copies are then processed with the reference signal using CAF, and arranged in a similar manner to form a column vector. This process is repeated for each Doppler frequency unit. Consequently, this forms the measurement matrix $\mathbf{B}_S \in \mathbb{C}^{LM \times LM}$, expressed as

$$\mathbf{B}_S = [\chi_{1,1} \chi_{1,2} \cdots \chi_{1,L} \chi_{2,1} \cdots \chi_{m,l} \cdots \chi_{M,L}] \tag{9}$$

where $\chi_{m,l}$ represents a copy of the CAF obtained by adding the delay τ_l and Doppler frequency f_{dm} to the reference signal. It can be expressed as follows:

$$\chi_{m,l} = \begin{bmatrix} \chi_{m,l}(\tau_1, f_{d1}) \chi_{m,l}(\tau_2, f_{d1}) \cdots \chi_{m,l}(\tau_L, f_{d1}) \chi_{m,l}(\tau_1, f_{d2}) \\ \cdots \chi_{m,l}(\tau_1, f_{dM}) \cdots \chi_{m,l}(\tau_L, f_{dM}) \end{bmatrix}^T \tag{10}$$

The sparse vector $\sigma_{m,l}$ formed by the amplitude gains $\sigma_S \in \mathbb{C}^{LM \times 1}$ can be expressed as

$$\sigma_S = [\sigma_{1,1} \sigma_{1,2} \cdots \sigma_{1,L} \sigma_{2,1} \cdots \sigma_{m,l} \cdots \sigma_{M,L}]^T \tag{11}$$

Therefore, \mathbf{a}_S can be expressed as

$$\mathbf{a}_S = \mathbf{B}_S \sigma_S + \mathbf{n} \tag{12}$$

where $\mathbf{n} \in \mathbb{C}^{LM \times 1}$ represents the impact of noise on CAF.

Equation (12) represents the sparse representation model of CAF. However, when the delay-Doppler domain is large, the size of the measurement matrix \mathbf{B}_S becomes large, imposing high computational and memory resource requirements. Therefore, we propose improvements to the sparse representation model to reduce computational and memory resource usage.

Let the CAF matrix $\mathbf{A}_S \in \mathbb{C}^{L \times M}$ be the rearranged form of CAF $\chi(\tau, f_d)$ before being organized into the column vector \mathbf{a}_S , i.e.,

$$\mathbf{A}_S = \begin{bmatrix} \chi(\tau_1, f_{d1}) & \chi(\tau_1, f_{d2}) & \cdots & \chi(\tau_1, f_{dM}) \\ \chi(\tau_2, f_{d1}) & \chi(\tau_2, f_{d2}) & \cdots & \chi(\tau_2, f_{dM}) \\ \vdots & \vdots & \ddots & \vdots \\ \chi(\tau_L, f_{d1}) & \chi(\tau_L, f_{d2}) & \cdots & \chi(\tau_L, f_{dM}) \end{bmatrix} \tag{13}$$

A_S is divided into $R \times C$ equally sized sub-blocks, each with dimensions $L' \times M'$, where $L = RL'$ and $M = CM'$. Then, A_S can be expressed as

$$A_S = \begin{bmatrix} A_{S,1,1} & A_{S,1,2} & \cdots & A_{S,1,C} \\ A_{S,2,1} & A_{S,2,2} & \cdots & A_{S,2,C} \\ \vdots & \vdots & \ddots & \vdots \\ A_{S,R,1} & A_{S,R,2} & \cdots & A_{S,R,C} \end{bmatrix} \quad (14)$$

Without loss of generality, consider the case where, for any $r \in \{1, 2, \dots, R\}$, and $c \in \{1, 2, \dots, C\}$, there are targets present in the (r, c) -th sub-block $A_{S,r,c} \in \mathbb{C}^{L' \times M'}$. Let $\{\tau_{r,c,1}, \tau_{r,c,2}, \dots, \tau_{r,c,L'}\}$ and $\{f_{r,c,1}, f_{r,c,2}, \dots, f_{r,c,M'}\}$ represent the delay and Doppler frequency corresponding to $A_{S,r,c}$. Then, $A_{S,r,c}$ can be expressed as

$$A_{S,r,c} = \begin{bmatrix} \chi(\tau_{r,c,1}, f_{r,c,1}) & \chi(\tau_{r,c,1}, f_{r,c,2}) & \cdots & \chi(\tau_{r,c,1}, f_{r,c,M'}) \\ \chi(\tau_{r,c,2}, f_{r,c,1}) & \chi(\tau_{r,c,2}, f_{r,c,2}) & \cdots & \chi(\tau_{r,c,2}, f_{r,c,M'}) \\ \vdots & \vdots & \ddots & \vdots \\ \chi(\tau_{r,c,L'}, f_{r,c,1}) & \chi(\tau_{r,c,L'}, f_{r,c,2}) & \cdots & \chi(\tau_{r,c,L'}, f_{r,c,M'}) \end{bmatrix} \quad (15)$$

Let $\mathbf{a}_{S,r,c} \in \mathbb{C}^{L'M' \times 1}$ be the column vector form of $A_{S,r,c}$, i.e.,

$$\mathbf{a}_{S,r,c} = \begin{bmatrix} \chi(\tau_{r,c,1}, f_{r,c,1}) \chi(\tau_{r,c,2}, f_{r,c,1}) \cdots \chi(\tau_{r,c,L'}, f_{r,c,1}) \chi(\tau_{r,c,1}, f_{r,c,2}) \\ \cdots \chi(\tau_{r,c,L'}, f_{r,c,m'}) \cdots \chi(\tau_{r,c,L'}, f_{r,c,M'}) \end{bmatrix}^T \quad (16)$$

The measurement matrix $\mathbf{B}_{S,r,c} \in \mathbb{C}^{L'M' \times L'M'}$ corresponding to $\mathbf{a}_{S,r,c}$ is expressed as

$$\mathbf{B}_{S,r,c} = \begin{bmatrix} \chi_{1,1}^{r,c} \chi_{1,2}^{r,c} \cdots \chi_{1,L'}^{r,c} \chi_{2,1}^{r,c} \cdots \chi_{m',l'}^{r,c} \cdots \chi_{M',L'}^{r,c} \end{bmatrix} \quad (17)$$

where $\chi_{m',l'}^{r,c} \in \mathbb{C}^{L'M' \times 1}$ represents a copy of the CAF obtained by adding the delay $\tau_{r,c,l'}$ and Doppler frequency $f_{r,c,m'}$ to the reference signal. It can be expressed as

$$\chi_{m',l'}^{r,c} = \begin{bmatrix} \chi_{m',l'}(\tau_{r,c,1}, f_{r,c,1}) \chi_{m',l'}(\tau_{r,c,2}, f_{r,c,1}) \\ \cdots \chi_{m',l'}(\tau_{r,c,L'}, f_{r,c,1}) \chi_{m',l'}(\tau_{r,c,1}, f_{r,c,2}) \\ \cdots \chi_{m',l'}(\tau_{r,c,l'}, f_{r,c,m'}) \cdots \chi_{m',l'}(\tau_{r,c,L'}, f_{r,c,M'}) \end{bmatrix}^T \quad (18)$$

From (7) and (18), it can be observed that the peak position of the CAF copy $\chi_{m',l'}^{r,c}$ is only related to m' and l' , and is independent of r and c . Therefore, when performing sparse recovery for each $\mathbf{a}_{S,r,c}$, the measurement matrix $\mathbf{B}_{S,r,c}$ can be reused. In other words, after obtaining $\mathbf{B}_{S,1,1}$, for any r and c , use $\mathbf{B}_{S,1,1}$ instead of $\mathbf{B}_{S,r,c}$.

However, as constructing $\mathbf{B}_{S,1,1}$ requires calculating $L'M'$ CAFs, even constructing only $\mathbf{B}_{S,1,1}$ involves a huge computational load. For any m' and l' , the difference between different CAF copies $\chi_{m',l'}^{r,c}$ lies only in the different peak positions. Therefore, we propose a method of self ambiguity function cropping to construct the measurement matrix $\mathbf{B}_{S,1,1}$ and reduce the computational load.

Let the self ambiguity function of the reference signal $u_{ref}(t)$ be $\chi_{ref}(\tau, f_d)$, i.e.,

$$\chi_{ref}(\tau, f_d) = \int_0^T u_{ref}^*(t - \tau) u_{ref}(t) e^{-j2\pi f_d t} dt \quad (19)$$

Suppose the matrix $\mathbf{A}_{ref} \in \mathbb{C}^{(2L'M'-1) \times (2L'M'-1)}$ formed by χ_{ref} corresponds to the delay and Doppler frequency $\{\tau_{-L'+1}^{ref}, \tau_{-L'+2}^{ref}, \dots, \tau_{L'-1}^{ref}\}$, and $\{f_{-M'+1}^{ref}, f_{-M'+2}^{ref}, \dots, f_{M'-1}^{ref}\}$, where $(\tau_0^{ref}, f_0^{ref}) = (0, 0)$. Then, \mathbf{A}_{ref} can be expressed as

$$\mathbf{A}_{ref} = \begin{bmatrix} \chi_{ref}(\tau_{-L'+1}^{ref}, f_{-M'+1}^{ref}) & \chi_{ref}(\tau_{-L'+1}^{ref}, f_{-M'+2}^{ref}) & \cdots & \chi_{ref}(\tau_{-L'+1}^{ref}, f_{M'-1}^{ref}) \\ \chi_{ref}(\tau_{-L'+2}^{ref}, f_{-M'+1}^{ref}) & \chi_{ref}(\tau_{-L'+2}^{ref}, f_{-M'+2}^{ref}) & \cdots & \chi_{ref}(\tau_{-L'+2}^{ref}, f_{M'-1}^{ref}) \\ \vdots & \vdots & \ddots & \vdots \\ \chi_{ref}(\tau_{L'-1}^{ref}, f_{-M'+1}^{ref}) & \chi_{ref}(\tau_{L'-1}^{ref}, f_{-M'+2}^{ref}) & \cdots & \chi_{ref}(\tau_{L'-1}^{ref}, f_{M'-1}^{ref}) \end{bmatrix} \quad (20)$$

Let the matrix form of the CAF copy $\chi_{m',l'}^{1,1}$ be $\mathbf{X}_{m',l'}^{1,1} \in \mathbb{C}^{L' \times M'}$, then $\mathbf{X}_{m',l'}^{1,1}$ can be obtained by cropping from \mathbf{A}_{ref} , i.e.,

$$\mathbf{X}_{m',l'}^{1,1} = \begin{bmatrix} \chi_{ref}(\tau_{1-l'}^{ref}, f_{1-m'}^{ref}) & \chi_{ref}(\tau_{1-l'}^{ref}, f_{2-m'}^{ref}) & \cdots & \chi_{ref}(\tau_{1-l'}^{ref}, f_{M'-m'}^{ref}) \\ \chi_{ref}(\tau_{2-l'}^{ref}, f_{1-m'}^{ref}) & \chi_{ref}(\tau_{2-l'}^{ref}, f_{2-m'}^{ref}) & \cdots & \chi_{ref}(\tau_{2-l'}^{ref}, f_{M'-m'}^{ref}) \\ \vdots & \vdots & \ddots & \vdots \\ \chi_{ref}(\tau_{L'-l'}^{ref}, f_{1-m'}^{ref}) & \chi_{ref}(\tau_{L'-l'}^{ref}, f_{2-m'}^{ref}) & \cdots & \chi_{ref}(\tau_{L'-l'}^{ref}, f_{M'-m'}^{ref}) \end{bmatrix} \quad (21)$$

Therefore, $\chi_{m',l'}^{1,1}$ can be expressed as

$$\chi_{m',l'}^{1,1} = \begin{bmatrix} \chi_{ref}(\tau_{1-l'}^{ref}, f_{1-m'}^{ref}) & \chi_{ref}(\tau_{2-l'}^{ref}, f_{1-m'}^{ref}) \\ \cdots & \chi_{ref}(\tau_{L'-l'}^{ref}, f_{1-m'}^{ref}) & \chi_{ref}(\tau_{1-l'}^{ref}, f_{2-m'}^{ref}) \\ \cdots & \chi_{ref}(\tau_{L'-l'}^{ref}, f_{M'-m'}^{ref}) \end{bmatrix}^T \quad (22)$$

$\mathbf{B}_{S,1,1}$ can be expressed as

$$\mathbf{B}_{S,1,1} = [\chi_{1,1}^{1,1} \chi_{1,2}^{1,1} \cdots \chi_{1,L'}^{1,1} \chi_{2,1}^{1,1} \cdots \chi_{m',l'}^{1,1} \cdots \chi_{M',L'}^{1,1}] \quad (23)$$

So far, we have completed the rapid construction of the measurement matrix. To establish the sparse representation model, let $\sigma_{S,r,c} \in \mathbb{C}^{L'M' \times 1}$ be the sparse vector corresponding to the (r, c) -th sub-block, i.e.,

$$\sigma_{S,r,c} = [\sigma_{1,1}^{r,c} \sigma_{1,2}^{r,c} \cdots \sigma_{1,L'}^{r,c} \sigma_{2,1}^{r,c} \cdots \sigma_{m',l'}^{r,c} \cdots \sigma_{M',L'}^{r,c}]^T \quad (24)$$

Therefore, the sparse representation model for the (r, c) -th sub-block is given by

$$\mathbf{a}_{S,r,c} = \mathbf{B}_{S,1,1} \sigma_{S,r,c} + \mathbf{n}_{r,c} \quad (25)$$

where $\mathbf{n}_{r,c} \in \mathbb{C}^{L'M' \times 1}$ represents the impact of noise on the (r, c) -th sub-block.

Let the sparse matrix $\Sigma_{S,r,c} \in \mathbb{C}^{L' \times M'}$ be the matrix form of the sparse vector $\sigma_{S,r,c}$, i.e.,

$$\Sigma_{S,r,c} = \begin{bmatrix} \sigma_{1,1}^{r,c} & \sigma_{2,1}^{r,c} & \cdots & \sigma_{M',1}^{r,c} \\ \sigma_{1,2}^{r,c} & \sigma_{2,2}^{r,c} & \cdots & \sigma_{M',2}^{r,c} \\ \vdots & \vdots & \ddots & \vdots \\ \sigma_{1,L'}^{r,c} & \sigma_{2,L'}^{r,c} & \cdots & \sigma_{M',L'}^{r,c} \end{bmatrix} \quad (26)$$

Therefore, the sparse matrix $\Sigma_S \in \mathbb{C}^{L \times M}$ corresponding to the CAF matrix A_S is given by

$$\Sigma_S = \begin{bmatrix} \Sigma_{S,1,1} & \Sigma_{S,1,2} & \cdots & \Sigma_{S,1,C} \\ \Sigma_{S,2,1} & \Sigma_{S,2,2} & \cdots & \Sigma_{S,2,C} \\ \vdots & \vdots & \ddots & \vdots \\ \Sigma_{S,R,1} & \Sigma_{S,R,2} & \cdots & \Sigma_{S,R,C} \end{bmatrix} \quad (27)$$

Here, we have completed the rapid construction of the sparse representation model for CAF. The main steps are as follows:

1. Compute CAF for reference signal $u_{ref}(t)$ and surveillance signal $u_{surv}(t)$ to obtain A_S . Divide A_S into equally sized blocks: $A_{S,1,1} \cdots A_{S,R,C}$.
2. Transform the CAF blocks $A_{S,1,1} \cdots A_{S,R,C}$ into vector form, denoted as $a_{S,1,1} \cdots a_{S,R,C}$.
3. Compute the self ambiguity function for the reference signal $u_{ref}(t)$ to obtain A_{ref} . Crop A_{ref} to obtain CAF copies $X_{1,1}^{1,1} \cdots X_{M',L'}^{1,1}$.
4. Convert the CAF copies $X_{1,1}^{1,1} \cdots X_{M',L'}^{1,1}$ into vector form, i.e., $\chi_{1,1}^{1,1} \cdots \chi_{M',L'}^{1,1}$.
5. Join the vectorized CAF copies $\chi_{1,1}^{1,1} \cdots \chi_{M',L'}^{1,1}$ to obtain the measurement matrix $B_{S,1,1}$.
6. Use the measurement matrix $B_{S,1,1}$ to perform sparse recovery on the vectorized CAF blocks $a_{S,1,1} \cdots a_{S,R,C}$, to obtain sparse vectors $\sigma_{S,1,1} \cdots \sigma_{S,R,C}$.
7. Convert the sparse vectors $\sigma_{S,1,1} \cdots \sigma_{S,R,C}$ into matrix form, i.e., $\Sigma_{S,1,1} \cdots \Sigma_{S,R,C}$.
8. Join the sparse matrices $\Sigma_{S,1,1} \cdots \Sigma_{S,R,C}$ to obtain the sparse matrix Σ_S corresponding to A_S .

3.2. Target Detection Based on Sparse Recovery

The solution to sparse vectors requires sparse recovery. In recent years, many sparse recovery algorithms [36–44] have been applied to address this issue. However, these algorithms need the measurement matrix to satisfy the restricted isometry property (RIP) condition, and the verification of RIP condition is an NP-hard problem. Therefore, we employed a sparse recovery algorithm based on the l_0 pseudonorm iterative solution [45] to reduce the theoretical limitations. This algorithm uses the following pseudonorm as a replacement for the l_0 norm:

$$\|x\|_{g_\alpha} = \sum_{d=1}^D g_\alpha(x_d), \quad x \in \mathbb{R}^{D \times 1} \quad (28)$$

In (28), x_d represents the d -th element of x . Where $g_\alpha(x)$ is

$$g_\alpha(x) = \frac{|x|}{\sqrt{x^2 + \alpha}} \quad (29)$$

The relationship between $g_\alpha(x)$, x , and α is shown in Figure 4. Obviously, as α approaches 0, the properties of $g_\alpha(x)$ tend to 0 norm.

Because the domain of definition of $g_\alpha(x)$ is a set of real numbers, Equation (25) needs to be converted into real form.

$$\mathbf{a}_{r,c} = \begin{bmatrix} \text{Re}(\mathbf{a}_{S,r,c}) \\ \text{Im}(\mathbf{a}_{S,r,c}) \end{bmatrix} \quad (30)$$

$$\mathbf{B}_{1,1} = \begin{bmatrix} \text{Re}(\mathbf{B}_{S,1,1}) & -\text{Im}(\mathbf{B}_{S,1,1}) \\ \text{Im}(\mathbf{B}_{S,1,1}) & \text{Re}(\mathbf{B}_{S,1,1}) \end{bmatrix} \quad (31)$$

$$\boldsymbol{\sigma}_{r,c} = \begin{bmatrix} \text{Re}(\boldsymbol{\sigma}_{S,r,c}) \\ \text{Im}(\boldsymbol{\sigma}_{S,r,c}) \end{bmatrix} \quad (32)$$

In summary, based on (25) and (30)–(32), when the influence of noise is neglected, we have

$$\mathbf{a}_{r,c} = \mathbf{B}_{1,1} \boldsymbol{\sigma}_{r,c} \quad (33)$$

Therefore, as long as we obtain the sparse vector $\sigma_{r,c} \in \mathbb{R}^{2L'M' \times 1}$ and recover $\sigma_{S,r,c}$ from $\sigma_{r,c}$, the positions of the non-zero values in $\sigma_{S,r,c}$ can determine the cells in the (r,c) -th sub-block where the surveillance signal exists.

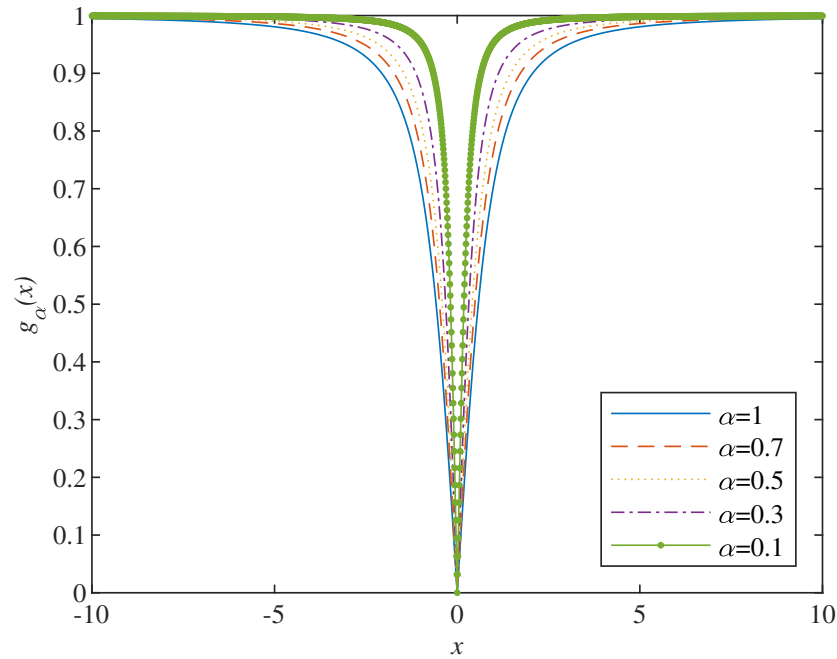


Figure 4. The relationship between $g_\alpha(x)$, x , and α . As α approaches 0, the properties of $g_\alpha(x)$ tend to 0 norm.

To estimate the sparse vector $\sigma_{r,c}$, consider the following problem

$$\begin{aligned} \min_{\sigma_{r,c} \in \mathbb{R}^{2L'M' \times 1}} \quad & \|\sigma_{r,c}\|_{g_\alpha} \\ \text{s.t.} \quad & \mathbf{a}_{r,c} = \mathbf{B}_{1,1} \sigma_{r,c} \end{aligned} \quad (34)$$

According to the derivation in reference [45], the expression for iteratively solving $\sigma_{r,c}$ can be obtained as

$$\sigma_{r,c} = \Gamma(\sigma_{r,c}) \mathbf{B}_{1,1}^T \left(\mathbf{B}_{1,1} \Gamma(\sigma_{r,c}) \mathbf{B}_{1,1}^T \right)^\dagger \mathbf{a}_{r,c} \quad (35)$$

where $\Gamma(\sigma_{r,c}) \in \mathbb{R}^{2L'M' \times 2L'M'}$ is a diagonal matrix, and its element at the i -th row and i -th column is given by

$$\Gamma(\sigma_{r,c})_{i,i} = \frac{|\sigma_{r,c,i}|}{g_\alpha'(\sigma_{r,c,i})} = \frac{|\sigma_{r,c,i}| \left(\sigma_{r,c,i}^2 + \alpha \right)^{1.5}}{\alpha} \quad (36)$$

where $\sigma_{r,c,i}$ is the i -th element of $\sigma_{r,c}$.

By analyzing (35), it can be observed that this equation is formulated as a fixed-point iteration. Performing a finite number of iterations on (35) yields the solution $\sigma_{r,c}^*$, indicating that the iteration is convergent.

4. Experimental Results

To validate the proposed approach for fast batches processing of sparse representation and recovery in the delay-Doppler domain, experiments are conducted using simulated and field signals with $\alpha = 0.1$. The experimental setup is as follows: first, the effectiveness of the proposed approach is verified using simulated signals. Second, the proposed approach is further validated by detecting two ship targets. Finally, a comparison of the real multiplication times is performed between the traditional and the proposed approach to highlight its computational efficiency advantage.

4.1. Simulation Results

Simulations are conducted using a DVB-T signal in 2K mode with quadrature phase shift keying (QPSK) as the symbol mapping scheme. The simulation parameters are presented in Table 1.

Table 1. Simulation Parameters.

Parameters	Values	Parameters	Values
Carrier frequency	600 MHz	Target 1 RCS	1 m ²
Sample rate	10 MHz	Target 2 RCS	10 m ²
Integration time	0.25 s	Target 3 RCS	5 m ²
IO coordinate	(200 km, 0, 0.15 km)	Transmitter power	1 kW
PBR coordinate	(0, 0, 5 m)	Transmitter gain	12.5 dB
Target 1 coordinate	(80 km, 20.1 km, 9.9 km)	Receiver gain	16 dB
Target 2 coordinate	(80 km, 20 km, 10 km)	Receiver bandwidth	10 MHz
Target 3 coordinate	(100 km, −23 km, 10 km)	Receiver temperature	298.15 K
Target 1 velocity	(45 m/s, 96 m/s, 0)		
Target 2 velocity	(50 m/s, 80 m/s, 0)		
Target 3 velocity	(70 m/s, 30 m/s, 0)		

Based on the parameters in Table 1, the delay for Target 1 and Target 2 are both 17.1 μs, while the delay for Target 3 is 20.6 μs. The Doppler frequencies of Target 1, Target 2, and Target 3 are −76.3 Hz, −62.7 Hz, and 26.8 Hz, respectively. Therefore, the delay for Targets 1 and 2 are the same, and their Doppler frequencies are close. The CAF result of the simulated signals is shown in Figure 5. It can be observed that all three targets appear in the delay-Doppler domain. Among them, Target 1 and Target 2 are closely located in the delay-Doppler domain, indicating the need for the separation of the two targets.

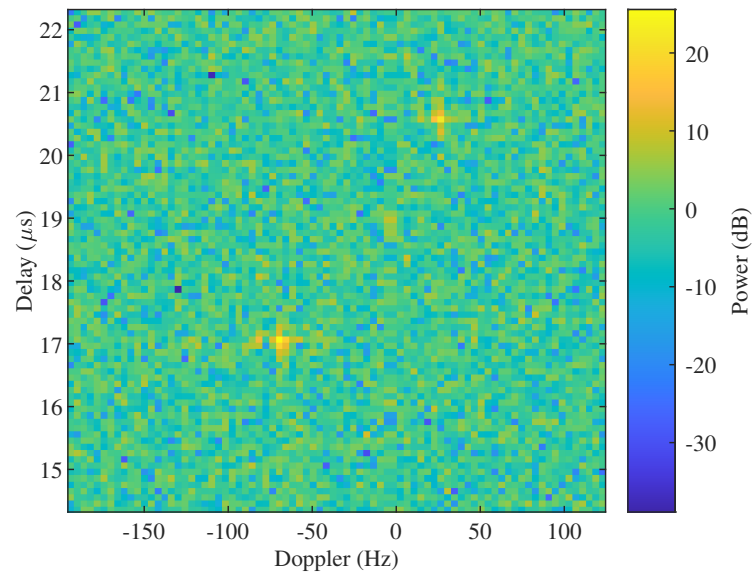


Figure 5. The CAF result of the simulated signals.

As the 13 dB detection threshold can guarantee a detection probability of 90% and a false alarm probability of 10^{-6} , the iterative initial value $\sigma_{r,c}^0 \in \mathbb{R}^{2L'M' \times 1}$ is set as

$$\sigma_{r,c}^0 = \begin{bmatrix} \sigma_{S,r,c}^0 \\ \mathbf{0}^{L'M' \times 1} \end{bmatrix} \quad (37)$$

where the elements of $\sigma_{S,r,c}^0 \in \mathbb{R}^{L'M' \times 1}$ corresponding to values greater than 13 dB in $\mathbf{a}_{S,r,c}$ are set to 1, and all other elements are set to 0. When $\sigma_{S,r,c}^0 = \mathbf{0}^{L'M' \times 1}$, the sparse recovery

operation is not performed on the (r, c) -th CAF block. In other words, the iterative result is $\sigma_{r,c}^* = \mathbf{0}^{2L'M' \times 1}$.

Under different values of R and C , the sparse recovery results of the simulated signals are shown in Figure 6.

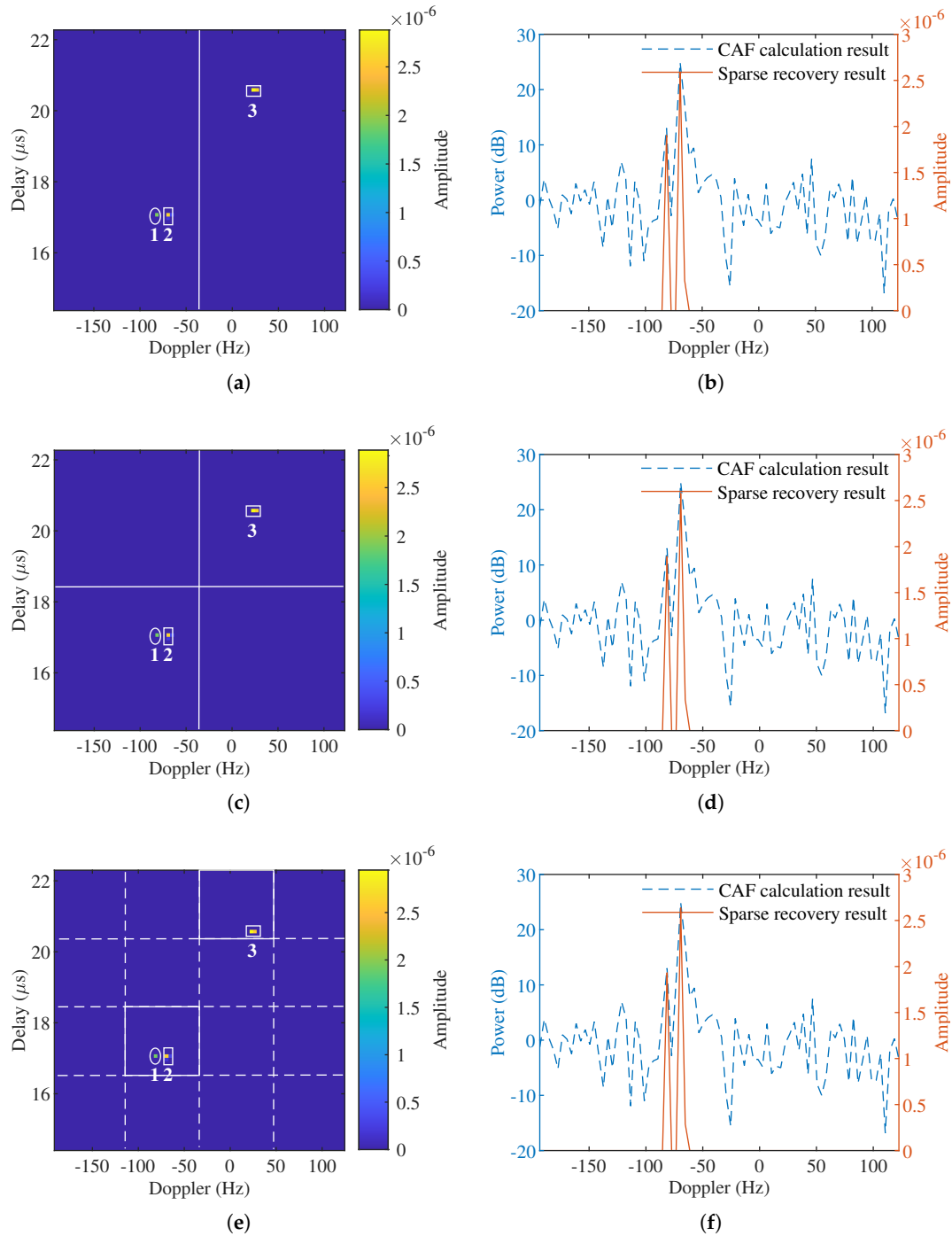


Figure 6. The sparse recovery results of the simulated signals. (a) Sparse recovery result with $R = 1, C = 2$. (b) Doppler frequency direction of the sparse recovery result with $R = 1, C = 2$. (c) Sparse recovery result with $R = 2, C = 2$. (d) Doppler frequency direction of the sparse recovery result with $R = 2, C = 2$. (e) Sparse recovery result with $R = 4, C = 4$. (f) Doppler frequency direction of the sparse recovery result with $R = 4, C = 4$.

From Figure 6, it can be observed that under different sub-block partitioning schemes, both Target 1 and Target 2 are separated in the delay-Doppler domain. Therefore, the sparse

recovery approach allows for the detection of weak targets, overcoming the influence of non-ideal factors from CAF.

4.2. Actual Test Results

In this section, the proposed approach is further validated using field signals. The field signals are obtained from reference [34] and collected using two Yagi-Uda antennas. One antenna is directed towards a DVB-T tower located in Sendai, Japan, and the other antenna is directed towards two ships entering the harbor. The signal has a carrier frequency of approximately 509 MHz, a sampling rate of 2.048 MHz, and an integration time of 0.07 s. To improve the experimental results of the field signal, the extensive cancellation algorithm (ECA) [46] is used for clutter suppression in the surveillance signal, and the radon fourier transform (RFT) [47] algorithm is used for motion compensation. The CAF result of the field signals is shown in Figure 7. It can be observed that the widening of the strong target peak covers the weak target peak in the Doppler domain, resulting in difficulties in detecting the weak target.

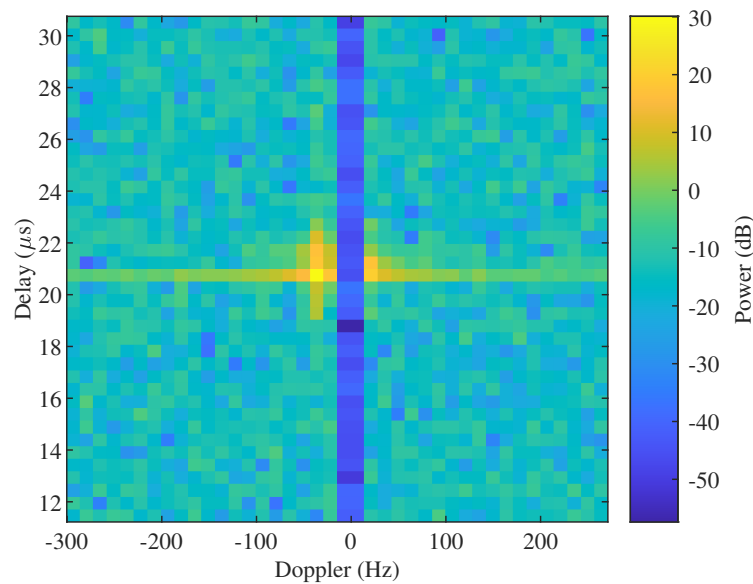


Figure 7. The CAF result of the field signals.

Under different values of R and C , the sparse recovery results of the field signals are shown in Figure 8.

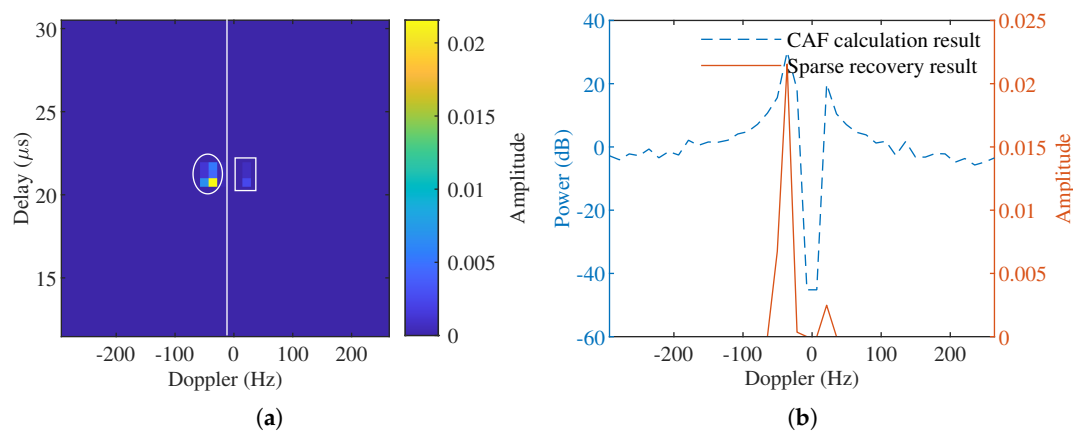


Figure 8. Cont.

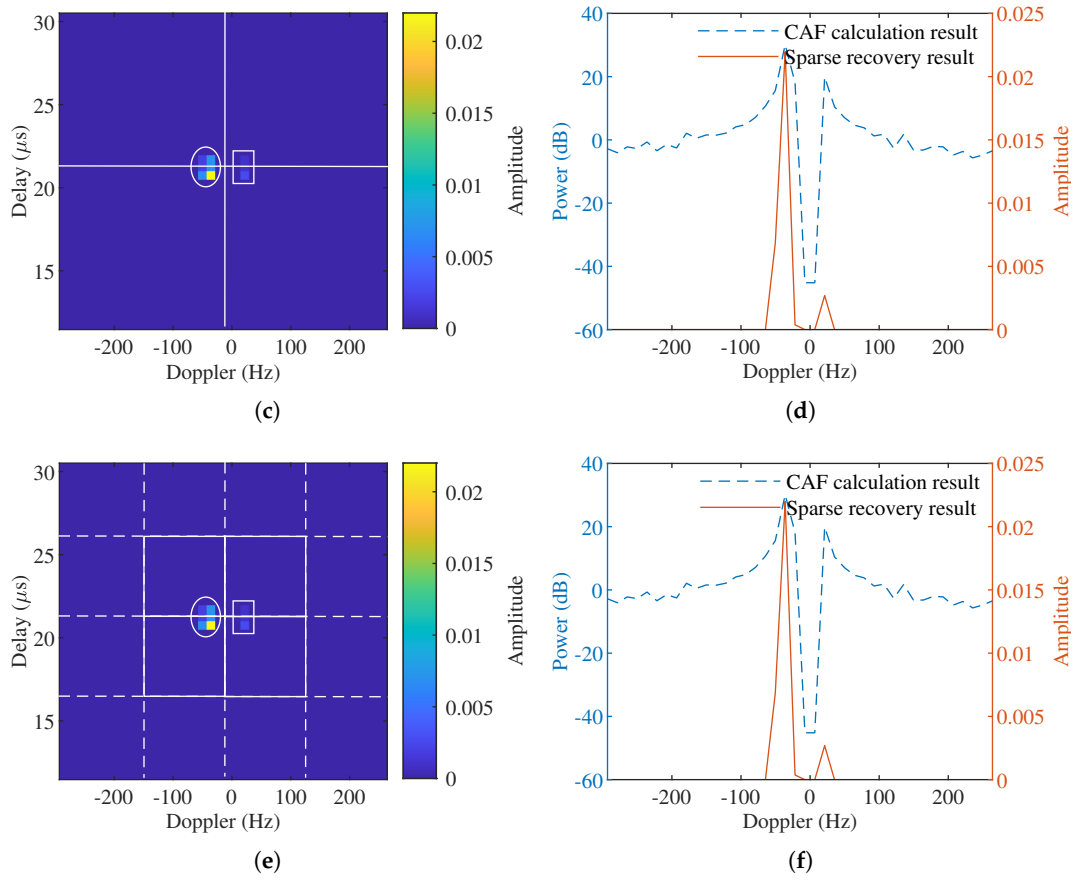


Figure 8. The sparse recovery results of the field signals. (a) Sparse recovery result with $R = 1, C = 2$. (b) Doppler frequency direction of the sparse recovery result with $R = 1, C = 2$. (c) Sparse recovery result with $R = 2, C = 2$. (d) Doppler frequency direction of the sparse recovery result with $R = 2, C = 2$. (e) Sparse recovery result with $R = 4, C = 4$. (f) Doppler frequency direction of the sparse recovery result with $R = 4, C = 4$.

As shown in Figure 8, under different sub-block partitioning schemes, the sparse recovery approach separates the two targets in the delay-Doppler domain. It enables the detection of the weak target without being affected by the non-ideal factors of CAF.

4.3. Comparison Results of Calculation Amount

In order to quantify the computational complexity of the proposed approach, we perform a theoretical calculation of the real multiplications for the traditional approach used in references [35] (i.e., (12)) and the optimized approach presented in this paper. For simplicity in the calculation, only cases where $L, M, L',$ and M' are powers of 2 are considered.

When the calculation of CAF employs the equivalent pulse compression method [7], according to the principles of the fast fourier transform (FFT), the number of real multiplications for CAF results of size $l \times m$ is given by

$$C_{CAF}(l, m) = 6m(2l - 1)\log_2(2l - 1) + 2ml\log_2(m) + 4m(2l - 1) \quad (38)$$

The number of real multiplications for the traditional sparse representation approach is

$$C_1 = (LM + 1)C_{CAF}(L, M) \quad (39)$$

The number of real multiplications for the optimized sparse representation approach is

$$C'_1 = C_{CAF}(L, M) + C_{CAF}(2L' - 1, 2M' - 1) \tag{40}$$

Based on the method of computing the Moore–Penrose pseudoinverse using singular value decomposition in Matlab, the number of real multiplications for sparse recovery of $l \times m$ -sized CAF results after k iterations is approximately

$$C_R(l, m) \approx k(40l^3m^3 + 16l^2m^2 + 12lm) \tag{41}$$

The number of real multiplications for sparse recovery using the traditional sparse representation approach is approximately

$$C_2 = C_R(L, M) \tag{42}$$

The number of real multiplications for sparse recovery using the optimized sparse representation approach is approximately

$$C'_2 = RCC_R(L', M') \tag{43}$$

Therefore, the number of real multiplications for the traditional sparse representation and recovery approach is approximately

$$C_{all} = C_1 + C_2 \tag{44}$$

The number of real multiplications for the optimized sparse representation and recovery approach is approximately

$$C'_{all} = C'_1 + C'_2 \tag{45}$$

Under different values of L , M , R , and C , we calculate the number of real multiplications for both the traditional and the optimized sparse representation approaches (according to (39) and (40)). The results are shown in Figure 9.

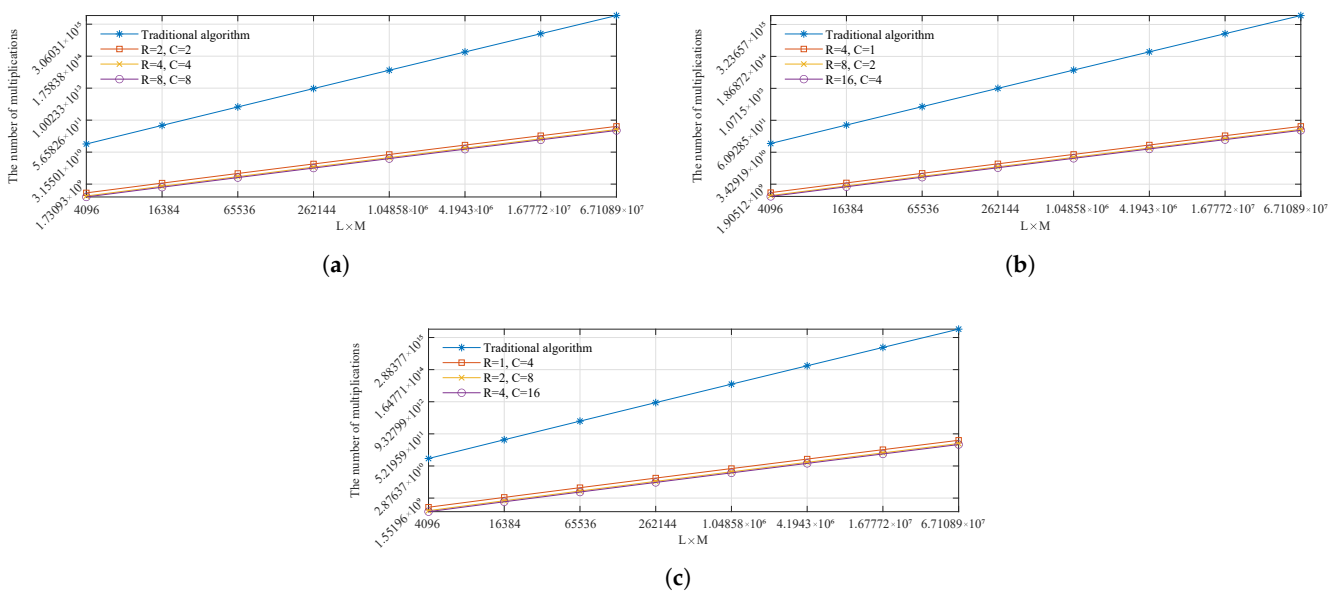


Figure 9. The number of real multiplications for the sparse representation approach. (a) $L = M$. (b) $L = 4M$. (c) $4L = M$.

From Figure 9, it can be observed that compared with the traditional sparse representation approach, the optimized sparse representation approach requires an order of

magnitude fewer real multiplications. Moreover, as L and M increase, the optimized sparse representation approach saves even more on the number of real multiplications.

Additionally, based on (44) and (45), we calculate the number of real multiplications for both the traditional and the optimized sparse representation and recovery approaches. The results are shown in Figure 10.

From Figure 10, it can be observed that when R and C are each doubled, the number of real multiplications decreases by approximately one order of magnitude. Therefore, for any sparse recovery approaches with a time complexity of $O(l^3 m^3)$, the optimization approach can play a similar role in reducing the computational complexity.

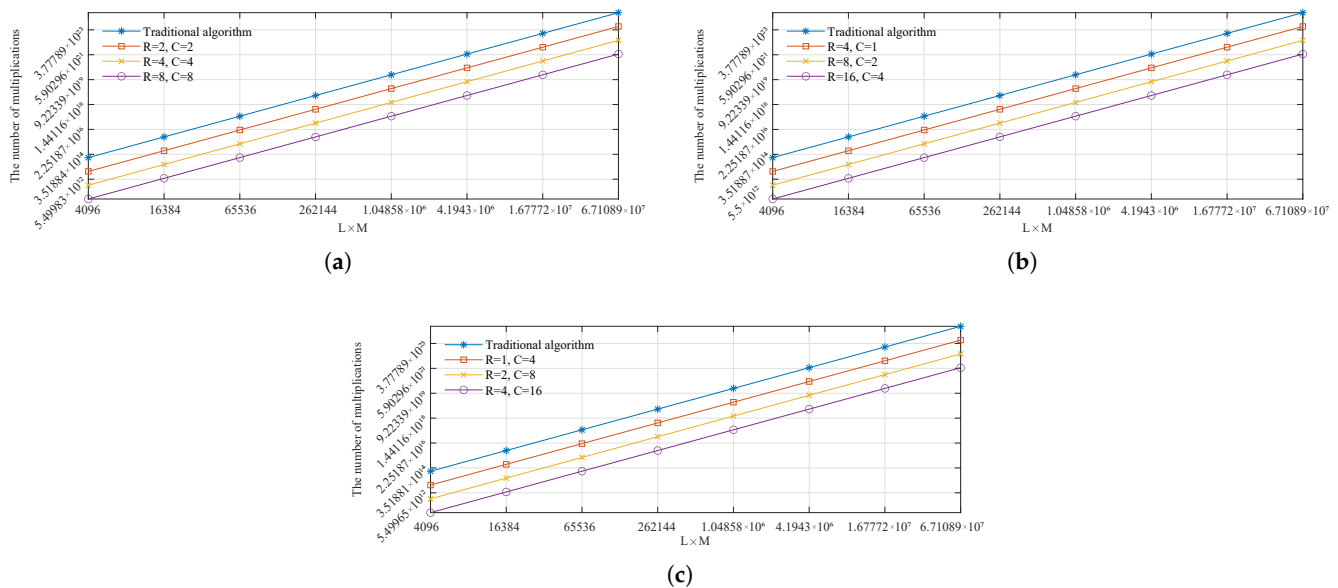


Figure 10. The number of real multiplications for the sparse representation and recovery approaches. (a) $L = M$. (b) $L = 4M$. (c) $4L = M$.

5. Conclusions

This paper addresses the challenges in detecting weak targets for PBR and the high computational demands of traditional sparse representation approaches. It proposes an PBR target detection model based on batch sparse representation and recovery. The model processes CAF into blocks, filters out blocks that require sparse representation and recovery based on whether targets exist in them, and improves the construction and utilization of the measurement matrix. Through the above processes, both weak target detection and computational efficiency are achieved. Compared with traditional approaches that rely on the sparsity of the delay-Doppler domain to detect weak targets, this approach requires fewer memory resources and computational complexity, while achieving an excellent weak target detection performance. In the sparse recovery process of CAF, the use of an iterative sparse recovery algorithm based on the l_0 pseudonorm avoids the challenge of verifying the RIP conditions, providing a more stable theoretical basis for the sparse recovery results. Experimental results demonstrate that, compared with the traditional approach, the proposed optimization approach achieves fast and stable detection of weak targets. As the number of blocks increases four-fold, the number of real multiplications decreases by approximately one order of magnitude. Therefore, the proposed optimization approach effectively realizes the fast and stable detection of weak targets. Furthermore, the sparse recovery for all blocks can be executed in parallel, laying the foundation for improving the algorithm's real-time performance.

Author Contributions: conceptualization, C.W.; methodology, K.C.; software, K.C.; formal analysis, K.C.; data curation, W.F.; writing—original draft preparation, K.C.; visualization, K.C. and C.W.; writing—review and editing, K.C. and C.W.; project administration, F.Z., C.L. and Y.G. All authors have read and agreed to the published version of the manuscript.

Funding: This research was funded by the National Natural Science Foundation of China, Grant Nos. 61631019, 61201418 and 62001350.

Data Availability Statement: The data that support this study are available from author W.F., upon reasonable request.

Acknowledgments: The authors thank the editors and anonymous reviewers for their help comments and suggestions.

Conflicts of Interest: The authors declare no conflicts of interest.

References

1. Zheng, H.; Wang, J.; Jiang, S.; Wu, X.; Gu, X. *Passive Bistatic Radar*, 1st ed.; National Defense Industry Press: Beijing, China, 2017.
2. Liu, R.; Dai, W.; Zhang, C. Multi-target Detection by Distributed Passive Radar Systems without Reference Signals. In Proceedings of the 2021 IEEE Wireless Communications and Networking Conference (WCNC), Nanjing, China, 29 March–1 April 2021; pp. 1–5.
3. Li, J.C.; Zhang, Y.D.; Zhang, Y.K.; Li, X.D. Direct Path Wave Purification for Passive Radar with Normalized Least Mean Square Algorithm. In Proceedings of the 2013 IEEE International Conference on Signal Processing, Communication and Computing (ICSPCC 2013), Kunming, China, 5–8 August 2013; pp. 1–4.
4. Yang, P.C.; Lyu, X.D.; Chai, Z.H.; Zhang, D.; Yue, Q.; Yang, J.M. Clutter Cancellation Along the Clutter Ridge for Airborne Passive Radar. *IEEE Geosci. Remote Sens. Lett.* **2017**, *14*, 951–955. [[CrossRef](#)]
5. Sui, J.; Wang, J.; Gao, J.; Fan, X. A Novel Strong Clutter Suppression Algorithm for Airborne Passive Radar. In Proceedings of the 2021 CIE International Conference on Radar (Radar), Haikou, China, 15–19 December 2021; pp. 2791–2794.
6. Moscardini, C.; Petri, D.; Capria, A.; Conti, M.; Martorella, M.; Berizzi, F. Batches algorithm for passive radar: A theoretical analysis. *IEEE Trans. Aerosp. Electron. Syst.* **2015**, *51*, 1475–1487. [[CrossRef](#)]
7. Rao, Y.; Nie, W.; Zhou, J. Fast Algorithm and Hardware Implementation of Ambiguity Function for Passive Radar. *Syst. Eng. Electron.* **2020**, *42*, 1953–1960.
8. Park, G.H.; Seo, Y.K.; Kim, H.N. Range-Doppler Domain-Based DOA Estimation Method for FM-Band Passive Bistatic Radar. *IEEE Access* **2020**, *8*, 56880–56891. [[CrossRef](#)]
9. Miao, Y.; Li, J.; Bao, Y.; Liu, F.; Hu, C. Efficient Multipath Clutter Cancellation for UAV Monitoring Using DAB Satellite-Based PBR. *Remote Sens.* **2021**, *13*, 3429. [[CrossRef](#)]
10. Gómez-del-Hoyo, P.J.; Jarabo-Amores, M.P.; Mata-Moya, D.; del-Rey-Maestre, N.; Rosa-Zurera, M. DVB-T Receiver Independent of Channel Allocation, With Frequency Offset Compensation for Improving Resolution in Low Cost Passive Radar. *IEEE Sens. J.* **2020**, *20*, 14958–14974. [[CrossRef](#)]
11. Zhang, X.; Yi, J.; Wan, X.; Liu, Y. Reference Signal Reconstruction Under Oversampling for DTMB-Based Passive Radar. *IEEE Access* **2020**, *8*, 74024–74038. [[CrossRef](#)]
12. Li, J. A DVB-S-Based Multichannel Passive Radar System for Vehicle Detection. *IEEE Access* **2021**, *9*, 2900–2912. [[CrossRef](#)]
13. Knoedler, B.; Steffes, C.; Koch, W. Detecting and Tracking a Small UAV in GSM Passive Radar Using Track-before-Detect. In Proceedings of the 2020 IEEE Radar Conference (RadarConf20), Florence, Italy, 21–25 September 2020; pp. 1–6.
14. Zhang, C.; Shi, S.; Yan, S.; Gong, J. Moving Target Detection and Parameter Estimation Using BeiDou GEO Satellites-Based Passive Radar with Short-Time Integration. *IEEE J. Sel. Top. Appl. Earth Obs. Remote Sens.* **2023**, *16*, 3959–3972. [[CrossRef](#)]
15. Zhang, Z.; Zheng, Y.; Zheng, L.; Zhu, P. Range Resolution and Sampling Frequency Trade-Off for GPS Passive Radar. *J. Syst. Eng. Electron.* **2022**, *33*, 28–37. [[CrossRef](#)]
16. Tao, R.; Gao, Z.; Wang, Y. Side Peaks Interference Suppression in DVB-T Based Passive Radar. *IEEE Trans. Aerosp. Electron. Syst.* **2012**, *48*, 3610–3619. [[CrossRef](#)]
17. Wang, T.; Liu, B.; Wang, X.; Xu, X.; Wei, Q. Passive radar analysis using DTMB signal. In Proceedings of the 2021 19th International Conference on Optical Communications and Networks (ICOON), Qufu, China, 23–27 August 2021; pp. 1–3.
18. Samczyński, P. 5G Network-Based Passive Radar. *IEEE Trans. Geosci. Remote Sens.* **2022**, *60*, 5108209. [[CrossRef](#)]
19. Zhang, X.; Labeau, F.; Liang, Y.C.; Fang, J. Compressive Sensing-Based Multiuser Detection via Iterative Reweighted Approach in M2M Communications. *IEEE Wirel. Commun. Lett.* **2018**, *7*, 764–767. [[CrossRef](#)]
20. Zhang, Y.; Xiang, Y.; Zhang, L.Y.; Rong, Y.; Guo, S. Secure Wireless Communications Based on Compressive Sensing: A Survey. *IEEE Commun. Surv. Tutor.* **2019**, *21*, 1093–1111. [[CrossRef](#)]
21. Lu, L.; Xu, W.; Wang, Y.; Tian, Z. Compressive Spectrum Sensing Using Sampling-Controlled Block Orthogonal Matching Pursuit. *IEEE Trans. Commun.* **2023**, *71*, 1096–1111. [[CrossRef](#)]
22. Chen, J.; Yang, J.G.; An, W.; Chen, Z.J. An Attitude Jitter Correction Method for Multispectral Parallax Imagery Based on Compressive Sensing. *IEEE Geosci. Remote Sens. Lett.* **2017**, *14*, 1903–1907. [[CrossRef](#)]

23. Li, H.; Dai, F.; Zhao, Q.; Ma, Y.; Cao, J.; Zhang, Y. Non-uniform Compressive Sensing Imaging Based on Image Saliency. *Chin. J. Electron.* **2023**, *32*, 159–165. [[CrossRef](#)]
24. Gan, H.; Shen, M.; Hua, Y.; Ma, C.; Zhang, T. From Patch to Pixel: A Transformer-Based Hierarchical Framework for Compressive Image Sensing. *IEEE Trans. Comput. Imaging* **2023**, *9*, 133–146. [[CrossRef](#)]
25. Wei, S. 3DRIED: A High-Resolution 3-D Millimeter-Wave Radar Dataset Dedicated to Imaging and Evaluation. *Remote Sens.* **2021**, *13*, 3366. [[CrossRef](#)]
26. Ajorloo, A.; Amini, A.; Amiri, R. A Joint Scheme of Antenna Placement and Power Allocation in a Compressive-Sensing-Based Colocated MIMO Radar. *IEEE Sens. Lett.* **2022**, *6*, 1–4. [[CrossRef](#)]
27. Zhu, L.; Wen, G.; Liang, Y.; Luo, D.; Jian, H. Multitarget Enumeration and Localization in Distributed MIMO Radar Based on Energy Modeling and Compressive Sensing. *IEEE Trans. Aerosp. Electron. Syst.* **2023**, *59*, 4493–4510. [[CrossRef](#)]
28. Berger, C.R.; Zhou, S.L.; Willett, P. Signal Extraction Using Compressed Sensing for Passive Radar with OFDM Signals. In Proceedings of the 2008 11th International Conference on Information Fusion, Cologne, Germany, 30 June–3 July 2008; pp. 1–6.
29. Zheng, L.; Wang, X. Super-Resolution Delay-Doppler Estimation for OFDM Passive Radar. *IEEE Trans. Signal Process.* **2017**, *65*, 2197–2210. [[CrossRef](#)]
30. Weiß, M. Compressive Sensing for Passive Surveillance Radar Using DAB Signals. In Proceedings of the 2014 International Radar Conference, Lille, France, 13–17 October 2014; pp. 1–6.
31. Hadi, M.A.; Tabassum, M.N.; Alshebeili, S. Compressive Sensing Based High-Resolution Passive Bistatic Radar. *Signal Image Video Process.* **2017**, *11*, 635–642. [[CrossRef](#)]
32. Nikaein, H.; Sheikhi, A.; Gazor, S. Target Detection in Passive Radar Sensors Using Least Angle Regression. *IEEE Sens. J.* **2021**, *21*, 4533–4542. [[CrossRef](#)]
33. Xie, D.; Yi, J.; Wan, X.; Jiang, H. Masking Effect Mitigation for FM-Based Passive Radar via Nonlinear Sparse Recovery. *IEEE Trans. Aerosp. Electron. Syst.* **2023**, *59*, 8246–8262. [[CrossRef](#)]
34. Feng, W.; Friedt, J.M.; Cherniak, G.; Sato, M. Batch Compressive Sensing for Passive Radar Range-Doppler Map Generation. *IEEE Trans. Aerosp. Electron. Syst.* **2019**, *55*, 3090–3102. [[CrossRef](#)]
35. Yang, P.C.; Lyu, X.D.; Li, J.C. Target Detection for Passive Radar Using Compressive Sensing. *Radar Sci. Technol.* **2015**, *13*, 384–389.
36. Yin, Q.; Yi, J.; Tang, J.; Zhu, Q. A Novel Orthogonal Matching Pursuit Algorithm based on Reduced-Dimension Dictionary for Airborne MIMO Radar. In Proceedings of the 2021 2nd International Symposium on Computer Engineering and Intelligent Communications (ISCEIC), Nanjing, China, 6–8 August 2021; pp. 202–206.
37. Ding, J.; Wang, M.; Kang, H.; Wang, Z. MIMO Radar Super-Resolution Imaging Based on Reconstruction of the Measurement Matrix of Compressed Sensing. *IEEE Geosci. Remote Sens. Lett.* **2022**, *19*, 3504705. [[CrossRef](#)]
38. Kulkarni, A.; Mohsenin, T. Low Overhead Architectures for OMP Compressive Sensing Reconstruction Algorithm. *IEEE Trans. Circuits Syst. Regul. Pap.* **2017**, *64*, 1468–1480. [[CrossRef](#)]
39. Vu, T.; Chunikhina, E.; Raich, R. On Local Linear Convergence Rate of Iterative Hard Thresholding for Matrix Completion. *IEEE Trans. Signal Process.* **2022**, *70*, 5940–5953. [[CrossRef](#)]
40. Cui, A.; He, H.; Xie, Z.; Yan, W.; Yang, H. Iterative Difference Hard-Thresholding Algorithm for Sparse Signal Recovery. *IEEE Trans. Signal Process.* **2023**, *71*, 1093–1102.
41. Matsumoto, N.; Mazumdar, A. Binary Iterative Hard Thresholding Converges with Optimal Number of Measurements for 1-Bit Compressed Sensing. In Proceedings of the 2022 IEEE 63rd Annual Symposium on Foundations of Computer Science (FOCS), Denver, CO, USA, 31 October–3 November 2022; pp. 813–822.
42. Liu, Y.; Zhan, Z.; Cai, J.F.; Guo, D.; Chen, Z.; Qu, X. Projected Iterative Soft-Thresholding Algorithm for Tight Frames in Compressed Sensing Magnetic Resonance Imaging. *IEEE Trans. Med. Imaging* **2016**, *35*, 2130–2140. [[CrossRef](#)]
43. Kim, D.; Park, D. Element-Wise Adaptive Thresholds for Learned Iterative Shrinkage Thresholding Algorithms. *IEEE Access* **2020**, *8*, 45874–45886. [[CrossRef](#)]
44. Chen, Y.; Sun, Y.; Liu, Q. Parametric Iterative Soft Thresholding Algorithm for Refocusing of Moving Targets in SAR Images. *IEEE Trans. Geosci. Remote Sens.* **2022**, *60*, 5229109. [[CrossRef](#)]
45. Wang, C.; Che, J.; Zhou, F.; Hou, J.; Li, C. Single Snapshot DOA Estimation by Minimizing the Fraction Function in Sparse Recovery. *Math. Probl. Eng.* **2020**, *2020*, 6163529. [[CrossRef](#)]
46. Del-Rey-Maestre, N.; Jarabo-Amores, M.P.; Bárcena-Humanes, J.L.; Mata-Moya, D.; Gómez-del-Hoyo, P. ECA Filter Effects on Ground Clutter Statistics in DVB-T Based Passive Radar. In Proceedings of the 2018 26th European Signal Processing Conference (EUSIPCO), Rome, Italy, 3–7 September 2018; pp. 1217–1221.
47. Zhou, X.; Wang, P.; Chen, J.; Men, Z.; Liu, W.; Zeng, H. A Modified Radon Fourier Transform for GNSS-Based Bistatic Radar Target Detection. *IEEE Geosci. Remote Sens. Lett.* **2022**, *19*, 3501805. [[CrossRef](#)]

Disclaimer/Publisher’s Note: The statements, opinions and data contained in all publications are solely those of the individual author(s) and contributor(s) and not of MDPI and/or the editor(s). MDPI and/or the editor(s) disclaim responsibility for any injury to people or property resulting from any ideas, methods, instructions or products referred to in the content.